Research on water status detection method of high-power fuel cell system based on water balance model

Yiyu Zhong[a], Yanbo Yang[a,b,*], Lipeng Diao[c], Naiyuan Yao[a], Tiancai Ma[a,b], Weikang Lin[a]

[a] *School of Automotive Studies, Tongji University, Shanghai, 201804, China*
[b] *Institute of Carbon Neutrality, Tongji University, Shanghai, 200092, China*
[c] *Beijing Electrical Research Institute, Beijing ,100070, China*

Abstract

With the gradually accelerating pace of global decarbonization, highly efficient and clean proton exchange membrane fuel cells(PEMFC) are considered one of the solutions for future energy. During the operation of the fuel cell, it is necessary to keep the internal proton exchange membrane in a good state of hydration, so an appropriate method of detecting the hydration state is essential. At present, the fuel cell system is rapidly developing towards high power, but the methods for detecting the hydration state of high-power fuel cell systems are still relatively lacking. Therefore, this paper studies the hydration state of high-power fuel cell systems and builds a condensation tail gas water collection device for calculating the water flow out of the fuel cell system. To verify the water balance model, a controlled variable experiment was conducted on a 100kW fuel cell system under different working temperatures, air metering ratios, and load currents. Finally, based on the experimental data, the change rate of the internal water content of the fuel cell system under different conditions was calculated. The results show that, under the same load current, as the working temperature and air metering ratio increase, the change rate of the internal water content of the fuel cell system gradually decreases. Therefore, at low power, it is necessary to maintain an appropriate working temperature, while at high power, maintaining an appropriate metering ratio is more important.

Keywords: PEMFC, water content, water balance, high power fuel cell system

1. Introduction

Proton exchange membrane fuel cells (PEMFCs), henceforth denoted as fuel cells, facilitate the direct conversion of chemical energy present in hydrogen into electrical energy. These fuel cells are characterized by their high energy utilization rate, low operating temperature, and the production of water as the sole reaction byproduct. Their versatility allows them to function not only as a small-scale distributed power supply

---

*Corresponding author

but also as the energy source for high-power transportation systems, thus demonstrating their broad applicability [1] . Nevertheless, the reliability, stability, and durability of the fuel cell stack, as the central component of the fuel cell power system, have emerged as critical factors influencing the extensive commercialization of fuel cell products. During the operation of the fuel cell, it is crucial to maintain the proton exchange membrane (PEM) in an optimal state of hydration to ensure that the proton conduction capability is at its zenith, thereby facilitating efficient and stable output performance. Hydration state failure is the most common failure mode in fuel cells, representing approximately half of total failures, and is primarily characterized by conditions of drying and flooding. Short-term hydration state failures can lead to fluctuations and reductions in the fuel cell's output performance, and if such conditions are prolonged, they may result in irreversible performance degradation. The deficiency of water in PEMFC can lead to a decrease in proton conductivity, as noted in the literature [2–4], which underscores the importance of monitoring and managing the hydration state to prevent operational inefficiencies and long-term damage to the fuel cell system.

In the event of a dry failure, the water content within the fuel cell stack is insufficient to maintain a properly hydrated state, leading to an increase in internal resistance and elevated heat production due to regions of the PEM not being fully hydrated. Prolonged dry conditions can potentially cause mechanical damage to the PEM, resulting in irreversible harm [5]. This highlights the critical need for maintaining adequate water content to prevent performance degradation and structural integrity loss in the fuel cell system. In the event of a flood failure, the water content inside the stack is too high, and the liquid water gradually block the flow channel or reaction area,preventing the reaction gas from reaching the reaction site, causing a local "starvation" phenomenon[6, 7]. In severe instances, additional side reactions can occur within the fuel cell under these conditions, leading to damage to the carbon carrier[7–9]. This emphasizes the importance of preventing extreme dry failures to safeguard the structural and functional integrity of the fuel cell components, thereby ensuring long-term reliability and performance.

In addition to the direct impact on output performance, the internal hydration state also indirectly affects environmental adaptability and durability[10, 11]. In low temperature conditions, especially in sub-zero environments, the free water inside the fuel cell will freeze, thereby blocking the reactant channels, and even causing structural damage to the catalyst layer and diffusion layer[12, 13]. In addition, it will also affect the aging characteristics of the catalyst[5, 14]. Flooding conditions will accelerate the loss of Pt surface area, while dry conditions will accelerate the corrosion of the carbon carrier [15, 16].

Research on fuel cell hydration states utilizes indicators like water content, electrical signals, and neutron imaging[17, 18], but high costs and complexity limit neutron imaging's adoption. Instead, the law of conservation of mass is employed to compute water content during stable operation, validated by comparing calculated rates with observed water distributions[19–21].

The output voltage of a fuel cell is a direct indicator of hydration state faults, influencing voltage fluctuations or drops, especially in high-power systems where the Cell Voltage Monitoring module (CVM) is a common standard[22, 23]. Electrical signal-based recognition standards, such as polarization curves and voltage fluctuation signals, show that severe water flooding leads to more pronounced voltage decay at higher cur-

2

rent densities [24]. Additionally, the pressure drop between the fuel cell's inlet and outlet, which increases with liquid water content, reflects water flooding severity and is diagnosed through various indicators and analysis methods[25].

The detection methods based on electrochemical signals mainly include electrochemical impedance spectroscopy, current interruption method, and cyclic voltammetry, etc. Among them, electrochemical impedance spectroscopy is the most common hydration state detection method because it can distinguish different electrochemical processes and can be tested online [15, 16]. As the air humidity decreases, the value of the high-frequency impedance segment (i.e., the intercept of the impedance spectrum with the real axis) gradually increases, the impedance spectrum moves to the right, and the radius of the low-frequency arc segment also gradually increases [17, 26, 27], which can be used as an indicator of the hydration state of the fuel cell.

When analyzing the relationship between impedance spectra and the internal hydration state of fuel cells, equivalent circuit models are often introduced. The model generally includes resistors, capacitors, inductors, and Warburg elements[28]. The model is capable of quantitatively analyzing the electrochemical process. The key to this method is the establishment of equivalent models and parameter identification. Fouquet et al.[25] extended the standard capacitor to a constant phase element, proving that the three resistance values of the model are related to the relative humidity of the air supply. Zhang et al.[26] used a neural network method to complete parameter identification, and the predicted Nyquist plot almost completely coincides with the measured value, and by directly predicting the parameters of the equivalent circuit, they detailed the degree of influence of different processes on fuel cell performance. BMW proposed a method for online monitoring of impedance, which requires collecting five frequency points, divided into three groups to fit the Randles circuit, obtaining ohmic impedance, polarization resistance and double layer capacitance[29].

However, the above methods are mostly suitable for single cells or low-power fuel cells. Applying them to high-power fuel cell doesn't gain any noticeable improvements[28, 30–33], since the assembly structure, flow field structure, and operating conditions of high-power fuel cell stacks are significantly different from those of single cells and low-power stacks [34].

Therefore, researchers have considered utilizing the law of conservation of mass to compute the water content within the fuel cell. When the fuel cell is operating stably, the flow rate of residual water can be calculated by measuring the discharged water. Zhao et al[35] employed a single transparent fuel cell to conduct tests under varying operating conditions. By comparing the calculated rate of change in water content within the fuel cell and the water distribution in the flow channel, the accuracy of the model was validated.

In addition, research has indicated that smaller-scale fuel cell stacks exhibit reduced sensitivity to gas flow rates[36], which can also cause the difference between small and big stacks.

Additionally, the variation in the number of cells within a fuel cell stack can significantly influence the power generation performance, leading to temperature imbalances[32]. This, in turn, further exacerbates the uneven distribution of water present throughout the stack. Consequently, there exists a pronounced distinction between smaller and larger stacks regarding these phenomena. Researches indicates that there may exist

notable differences in the water generation mechanisms between large-scale and small-scale proton exchange membrane fuel cell (PEMFC) stacks[37]. Therefore, traditional approaches relying on electrochemical analysis and similar techniques may not be applicable to large-scale stacks. Due to the fact that large-scale fuel cell stacks frequently operate at lower power densities[38], this could potentially have an impact on the water generation mechanisms involved, further differentiating them from their smaller-scale counterparts.

This study is dedicated to exploring the hydration state of high-power fuel cell systems and developing a validated water balance model. The research begins by examining the water balance model of a high-power fuel cell system and introduces a condensation-type exhaust water collection device to accurately measure the water flow rate exiting the system. To validate the constructed water balance model, controlled variable experiments were conducted across different operating temperatures, air-to-fuel ratios, and load currents. The experimental results show that with increasing operating temperature and air-to-fuel ratio, the water flow rate from the air side increases, while the water flow rate from the hydrogen side decreases. Additionally, as the load current increases, the water flow rate from both sides increases. Based on the experimental data, the rate of change in the internal water content of the fuel cell system under various conditions was calculated. The findings indicate that at the same load current, as the operating temperature and air stoichiometric ratio increase, the rate of change in the internal water content of the fuel cell system decreases. Conversely, as the load current increases, the influence of the air stoichiometric ratio also increases. Thus, at low power, maintaining an appropriate operating temperature is crucial, whereas at high power, managing an appropriate metering ratio becomes more significant. This research provides valuable insights into optimizing the operational parameters of high-power fuel cell systems to ensure efficient water management and system performance.

2. Experiment

To verify the reliability of the water balance model for high-power fuel cell systems, it is necessary to record the water-containing state of the high-power fuel cell system when it reaches water balance under different operating conditions. Therefore, the experimental conditions should meet the following three points:

- The selected operating parameters within normal operating range of the fuel cell system, reducing effects by faults in FC(Fuel Cell) system other than water content faults (gas supply insufficiency, air compressor surge, proportional valve failure, etc.)

- By designing experiments that manifest more pronounced phenomena under both dry and flooded conditions, the study would investigates the effects of water content faults in fuel cell systems.

- The steady-state operation time should be long enough to ensure that the water content inside the fuel cell is in dynamic balance during this period, avoiding the impact of dynamic characteristics on the experimental results.

Table 1: Water state experimental parameter table

Load current(A) / currency density(A·cm^{-2})	Working temperature(°C)	Air metering ratio
120/0.4	55,60,65,70,73	2,2.2,2.4,2.6,2.8
210/0.7	55,60,65,70,73	1.8,2,2.2,2.4
300/1.0	63,65,68,70,73	1.8,2,2.2,2.4

2.1. Experiment Design

Literature review highlights that the air-to-fuel ratio, operating temperature, and load current are the predominant factors affecting water content within the fuel cell[23]. Given the temperature inside stack can not be measured during operation, the inlet temperature of coolant is treated as working temperature in this research, and the working temperature in the following text refers to the inlet temperature of the coolant. According to the operating conditions recommended by the system side, a three-factor five-level water content experiment was designed. The parameters of the experiment are shown in Table 1.

Literatures[24] indicates that the time required for the fuel cell system to reach water balance is generally a few seconds to ten minutes. Therefore, each test point ran for 20 minutes, and it was assumed that the fuel cell was in the process of establishing water balance within the first 15 minutes, and no data was recorded for this process, and the data obtained in the last 5 minutes was recorded. During the test, if a single cell voltage is too low or other faults cause the fuel cell system to shut down, the data of this operating point will be removed.

2.2. Test platform introduction

The high-power fuel cell system used in this article is shown in Fig 1, manufactured by AT&M Environmental Engineering Technology Co. With rated net output power of 100kW, the stack is composed of 410 single cells. High-pressure dry hydrogen gas enters the anode of the reaction stack after being depressurized by the solenoid valve and proportional valve. The liquid water in the residual hydrogen is separated by the gas-water separation device and intermittently discharged through the drain valve.
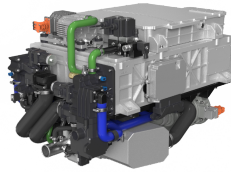

Figure 1: power system diagram

For the above fuel cell system, the water balance model can be represented as

$$\frac{dm_{w,sys}}{dt} = Q_{v,in,sys} + Q_{w,gen,ca} - Q_{w,out,ca} - Q_{w,out,an} \qquad (1)$$

In Formula (1), epresents the water

- $m_{(w,sys)}$ represents the water content inside the fuel cell system, in grams;

- $Q_{(v,in,sys)}$ represents the flow rate of water vapor entering the fuel cell system, in g/s;

- $Q_{(w,gen)}$ represents the water flow generated by the electrochemical reaction, in g/s;

- $Q_{(w,out,ca)}$ represents the water flow out of the system from the air subsystem, in g/s;

- $Q_{(w,out,an)}$ represents the water flow out of the system from the hydrogen subsystem, in g/s;

Taking the fuel cell system during steady-state operation as the research object, the change in the water content of the auxiliary system of the fuel cell system can be ignored, that is,

$$\frac{dm_{w,stk}}{dt} = \frac{dm_{w,sys}}{dt} \qquad (2)$$

Each part of the equation required for the water balance model is described below:

2.2.1. Water flow into the system

Since the hydrogen entering the system is high-pressure hydrogen with a purity of 99.99%, water vapor mainly enters the system with the air. By recording the temperature, humidity, pressure of the environment during the reaction process, and the air flow entering the system, the water flow entering the system can be calculated.

$$Q_{v,in,sys} = \frac{Q_{air;in,sys} \cdot P_{vamb} \cdot M_v}{M_a \cdot P_{amb}} = \frac{Q_{air;in,sys} \cdot (P_{amb} - P_{sat} * RH) \cdot M_v}{M_a \cdot P_{amb}} \qquad (3)$$

In Formula(3),

- $Q_{air;in,sys}$ stands for air flow into the system, in g/s;

- P_{amb} stands for environmental pressure, in kPa;

- R_v represents the relative humidity of the environment;

- P_{sat} represents the saturated vapor pressure of the environment, which can be calculated using the saturated water vapor pressure formula.

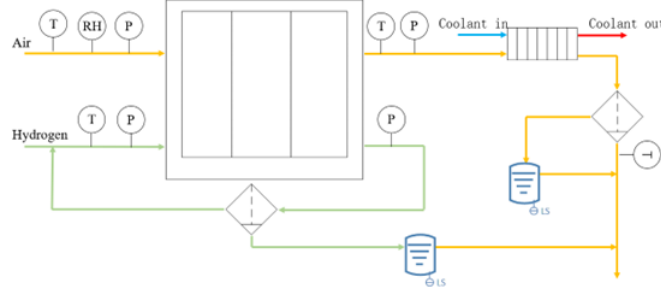$$p_{sat} = \exp\left(9.3876 - \frac{3826.36}{T_{amb} - 45.47}\right) \times 10^3 \qquad (4)$$

Figure 2: Schematic diagram of exhaust gas water content detection device

- T_{amb} represents environmental temperature, K;

- M_v represents water relative molecule mass, in g/mol;

- M_a represents water relative molecule mass, in g/mol;

Water flow by electrochemical reaction

The water flow produced by electrochemical reaction can be presented as formula below:

$$Q_{v,gen,ca} = \frac{N \cdot M_v \cdot I_{st}}{2F} \tag{5}$$

- N represents the number of single cells in the fuel cell stack.

- I_{st} represents load current, in A.

- F stands for faraday constant, which is 96485C/mol.

2.2.2. The water flow out of the system from the air side and the hydrogen side

To measure the water flow out of the system from the air and hydrogen sides, this article has designed an exhaust water content detection device centered on condensation. The exhaust water content detection device on the air side is composed of a heat exchanger, a water separator, a temperature sensor, and a water collection device with a liquid level sensor. The basic principle is to condense the high-temperature supersaturated exhaust gas on the air side, and then separate the liquid water inside from the exhaust gas through the water separator, thus obtaining saturated low-temperature exhaust gas and liquid water. Collect the separated liquid water and collect the liquid level with a liquid level sensor. Therefore, the water flow out of the system from the air side is composed of two parts: the liquid water collected in the air side collection device and the water vapor carried in the saturated steam after water vapor separation, that is,

$$Q_{w,out,ca} = \frac{dm_{w,cacollect}}{dt} + \frac{Q_{air,out,sys} \cdot p_{v,sat} \cdot M_v}{M_a \cdot P_{amb}} \tag{6}$$

In Formula(6),

- $m_{w,cacollect}$ represents the mass of the liquid collected by the exhaust water collection device on the air side, in grams(g);

- $Q_{air,out,sys}$ represents the air flow out of the system, in g(gram)/s(second), which can be calculated by the following formula.

The $Q_{air,out,sys}$ is represented as below:

$$Q_{air,outsys} = Q_{air,in,sys} - Q_{o,recat,ca} + Q_{v,gen,ca} - \frac{dm_{w,cacolect}}{dt} \qquad (7)$$

Since the hydrogen return circuit of the system is equipped with a water separator, the water content detection device on the hydrogen side mainly collects liquid water and a small amount of hydrogen, with less gaseous water, which does not significantly affect the experimental results. Therefore, the exhaust water content detection device on the hydrogen side only has a water collection device with a liquid level sensor, which is used to record the water flow discharged from the hydrogen side.

$$Q_{w,out,an} = \frac{dm_{w,ancollect}}{dt} \qquad (8)$$

$m_{w,ancollect}$ represents the mass of the liquid collected by the exhaust water collection device on the hydrogen side, in grams(g).

2.2.3. Test methods

In sequence, turn on host computer, system controller, electronic load, auxiliary devices, and impedance testing system; Turn on the water pump, solenoid valve, proportional valve, back pressure valve, air compressor, drain valve, and hydrogen circulation pump in sequence, setting the anode inlet gas pressure 10kPa higher than the cathode inlet gas pressure ($\Delta p = 20kPa$).

Gradually load the system to 120A, adjust the speed of the air compressor and the opening angle of the back pressure valve, so that the air flow rate reaches the air metering coefficient of 2.8 corresponding to the target current, gradually raise the working temperature to $55 \pm 1°C$, and start the temperature closed-loop control program to maintain this temperature; After the working temperature is stable at $55 \pm 1°C$, start timing and run for a total of 15 minutes; Adjust the speed of the air compressor and the opening angle of the back pressure valve, so that the air metering ratio gradually decreases in the range of $2 \sim 2.8$ with a step size of 0.2; Raise the working temperature to $60 \pm 1°C$, $65 \pm 1°C$, $70 \pm 1°C$, $73 \pm 1°C$, repeat the testing phase and record the experimental data.

Load up to 210A, 300A, repeat all recording steps, until all operating points water content detection experiments are completed.

Gradually reduce the load to 0A, purging circuit with nitrogen, turn off the machine, and power down in sequence.

3. Results and discussion

3.1. Effect of operating temperature on water flow rate outflow from air side

Fig 3 shows the change in the water flow out of the air side at different working temperatures. As can be seen from the Fig 3a, as the temperature rises, the water content

in the air side exhaust gas generally shows an upward trend. The higher the temperature, the higher the saturation vapor pressure of the fuel cell. Under the same water content, the relative humidity will decrease at this time, which is equivalent to the generation of less liquid water inside the fuel cell, and the ability of the gas to carry water is improved. This change applies to both the air side and the hydrogen side, which is shown in Fig 4b and Fig 4c. Therefore, under the same other conditions, the water flow out of the fuel cell stack by the air increases with the increase in temperature, and more liquid water is collected by the air side exhaust gas collection device. [h]
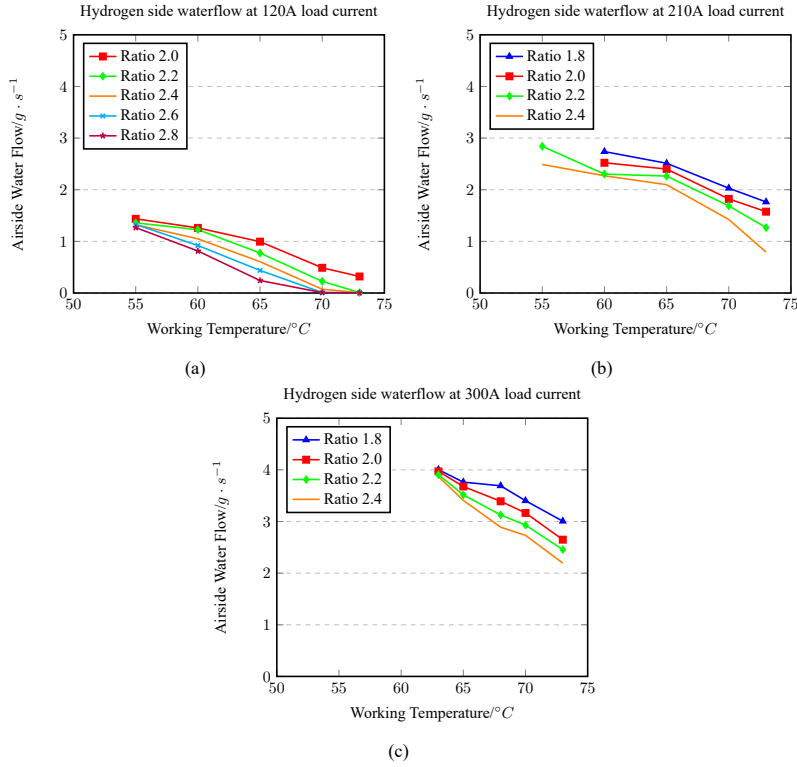

(a)

(b)

(c)

Figure 3: Comparison of water flow rate flowing out of the air side at different operating temperatures (a:120A; b:210A; c:300A; vertical water flow; horizontal as temperature; starting point from top to bottom is ordered by flow rate: 1.8/2.0/2.2/2.4)

It is worth noting that when the load current is 120A, the impact of the working temperature on the water flow of the air side is slightly different under different metering ratios. As the air metering ratio increases, the growth rate of the water flow on the air side gradually decreases. This is because at a small current density, the fuel cell produces less water due to the electrochemical reaction, and at the same time, the high-speed high-temperature reaction gas has a strong ability to carry water, and the water produced by the fuel cell has been completely carried out by the reaction gas. Therefore, even if the air metering ratio increases, the reaction gas cannot carry out more water. For the working conditions of low working temperature and large load current, the ability
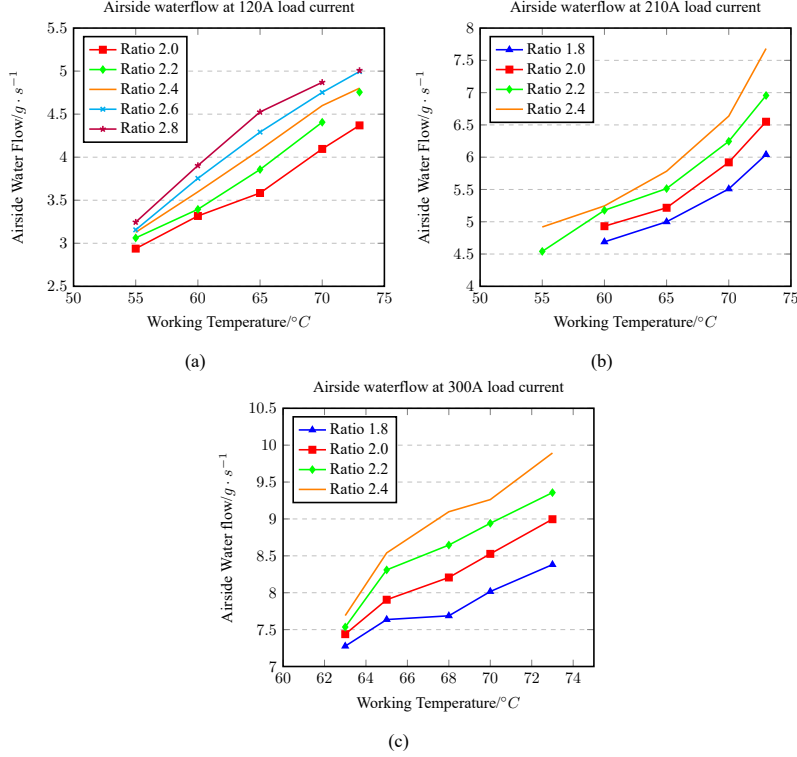
9

Figure 4: Comparison of water flow rate flowing out of the air side at different operating temperatures (a:120A; b:210A; c:300A; vertical water flow; horizontal as temperature; starting point from top to bottom is ordered by flow rate: 1.8/2.0/2.2/2.4)

of the reaction gas to carry water is low or the fuel cell produces more water, so there is still some water vapor or liquid water remaining in the system. At this time, if the air flow is increased, the water flow out of the system will also increase accordingly.

Fig 3a shows that as the temperature rises, the water content in the hydrogen side exhaust gas generally shows a downward trend, and even at $120A/70°C$, the water content in the hydrogen side exhaust gas is 0, the same result appears in 210A(Fig 3c) and 300A(Fig 3c). There are mainly two reasons for this phenomenon. First, according to the principle of proton exchange membrane fuel cell reaction, the reaction product water is generated at the cathode (that is, the air side), and the fuel used by the fuel cell system is 99.99% pure hydrogen. Therefore, the water inside the hydrogen side is mainly the water that migrates from the air side to the hydrogen side under the action of concentration diffusion and pressure diffusion. Since the hydrogen-air pressure difference is basically consistent (20kpa) during the experiment, the influence of pressure on water migration can be ignored when comparing. Second, the exhaust gas collected on the anode side needs to first pass through the water separator built into the fuel cell system to separate the unreacted hydrogen from the liquid water, and then it can be collected by the exhaust water collection device on the hydrogen side. And at higher

working temperatures, the saturation vapor pressure of the gas on the hydrogen side rises, and the content of liquid water decreases relatively. These two factors cause the working temperature to rise and the water content flowing out of the hydrogen side to decrease.

3.2. Influence of air metering ratio on the water flow out of the cathode and anode

Compare the water flow out of the air side and the hydrogen side at 120A, 210A, 300A load currents, different coolant inlet temperatures, and different air metering ratios, as shown in Fig 5a. Similar to the impact of working temperature on the water flow out of the air side, under the same load current, the higher the air metering ratio, the more water is carried out of the stack by the unreacted air, which also applies to load current of 210A(Fig 5b) and 300A(Fig 5c). It should be noted that this growth is not unlimited. After reaching a certain air metering ratio, the growth of the water content in the air side exhaust gas slows down, especially when the load current is small and the working temperature is high. This is because at this time, the water produced by the electrochemical reaction of the fuel cell has been completely carried out of the fuel cell by high-temperature high-speed air. At this time, even if the air metering ratio continues to increase, the water content of the exhaust gas will not continue to increase. [h]

For the hydrogen side, similarly, as the air metering ratio increases, the water flow out of the hydrogen side basically continues to decrease. After the above analysis, as the air metering ratio increases, the water stored in the cathode will be taken out of the stack by the high-speed airflow, and the water flow diffused to the hydrogen side through concentration difference becomes less, so relatively speaking, the water collected on the hydrogen side will become less. However, the degree of decline is different. Under low temperature (120A/60$°C$, 210A/60$°C$, and 300A/63$°C$), they all show a relatively gentle decline. As the temperature rises, the water flow out of the hydrogen side is also gradually affected by the air metering ratio.

3.3. Effects of operating temperature and air metering ratio on internal water content of fuel cell system

According to the working principle of the fuel cell, during the reaction process, water mainly comes from the electrochemical reaction and the water vapor that enters the fuel cell with the reaction gas. Then, a part of the water is discharged from the fuel cell with the exhaust gas after the reaction, and another part of the water stays inside the fuel cell. In this article, the change rate of the water remaining in the fuel cell will be used as the research object to evaluate the water content status inside the fuel cell.

$$\frac{dm_{w,stk}}{dt} = Q_{w,in,sys} + Q_{w,gen} - Q_{w,out,ca} - Q_{w,out,an} \tag{9}$$

In Formula 9, $m_{(w,stk)}$ is the water content inside the fuel cell, in g, $Q_{(w,in,sys)}$ is the water flow rate entering the fuel cell system, in (g/s), $Q_{(w,gen)}$ represents the water flow rate generated by the electrochemical reaction, in (g/s), $Q_{(w,out,ca)}$ represents the water flow rate flowing out of the system from the cathode, in (g/s), $Q_{(w,out,an)}$ represents the water flow rate flowing out of the system from the anode, in (g/s).
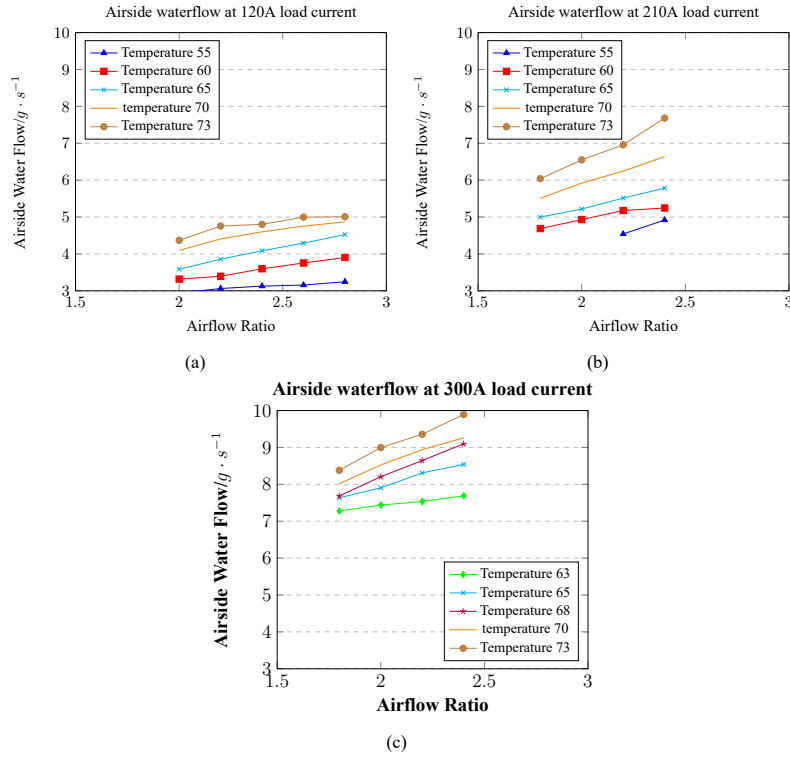
11

Figure 5: Comparison of water flow rate flowing out of the air side under different air metering ratios (a:120A; b:210A; c:300A; vertical as water flow; horizontal as air flow rate; starting point from top to bottom is ordered by temperature: 63/65/68/70/73°C)

Although during the reaction process, under the effects of concentration diffusion and electro-osmotic drag, water at the cathode will migrate to the anode. However, the research object of the water balance method is the entire fuel cell, so the internal water migration process will not have an impact.

Using the method described above, the rate of change of the water content inside the fuel cell system under different load currents, working temperatures, and air metering ratios can be calculated. In the process of making the graph, to maintain the integrity of the graph. We use (Load current/Temperature/Coefficient) as the format of test environment description. The data of (210A/55°C/1.8) and (210A/55°C/2.0) are replaced with (210A/55°C/2.2) test's data. The obtained results are compared as shown in Fig 7a, Fig 7b and Fig 7c, where positive values indicate an increase in water content (represented in blue), and negative values indicate a decrease in water content (represented in red). For the convenience of subsequent discussions, the blue part is defined as flooding, the red part is defined as drying, and the green part is defined as the normal state.

As can be seen from Fig 7, under the same load current, as the working temperature increases and the air metering ratio increases, the rate of change of the water
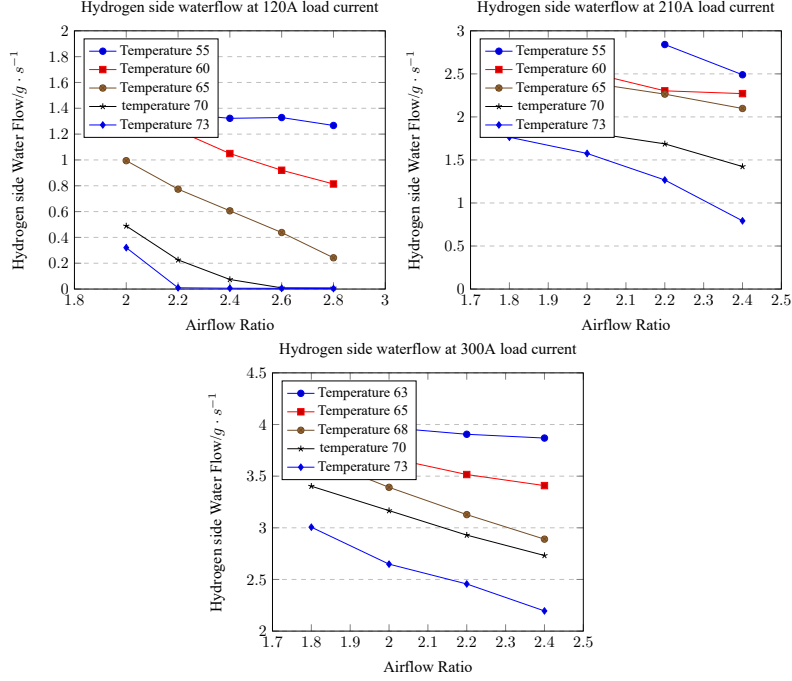
12

Figure 6: Comparison of water flow rate flowing out of the air side under different air metering ratios (a:120A; b:210A; c:300A; vertical as water flow; horizontal as air flow rate; starting point from top to bottom is ordered by temperature: 63/65/68/70/73℃)

content inside the fuel cell system gradually decreases. When it is (120A/73°C/2.8), (210A/73°C/2.4), (300A/73°C/2.4), the rate of change of the water content inside the fuel cell system reaches the minimum value under this load current. However, the degree of influence of the working temperature and the air metering ratio on the rate of change of the water content inside the fuel cell system is slightly different. When the load current is 120A and 210A, too low working temperature is more likely to cause flooding than too low air metering ratio. For example, at 120A, when the working temperature is 55°C, even if the air metering ratio reaches 2.8, the fuel cell system is still in a relatively flooded state; and when the working temperature is 73°C, even if the air metering ratio is only 2.0, the fuel cell system is in a normal state. In a dry state, the degree of influence of working temperature and air metering ratio is not much different. However, when the load current is 310A, the trend is the opposite. Too low working temperature and too low air metering ratio will cause flooding, and too high air metering ratio is more likely to cause drying than too high working temperature.

Furthermore, this paper uses the method of linear regression to analyze the impact of working temperature and air metering ratio on the water content inside the fuel cell system. Before this, the data needs to be standardized. This paper uses the Z-score normalization method[39, 40], which is
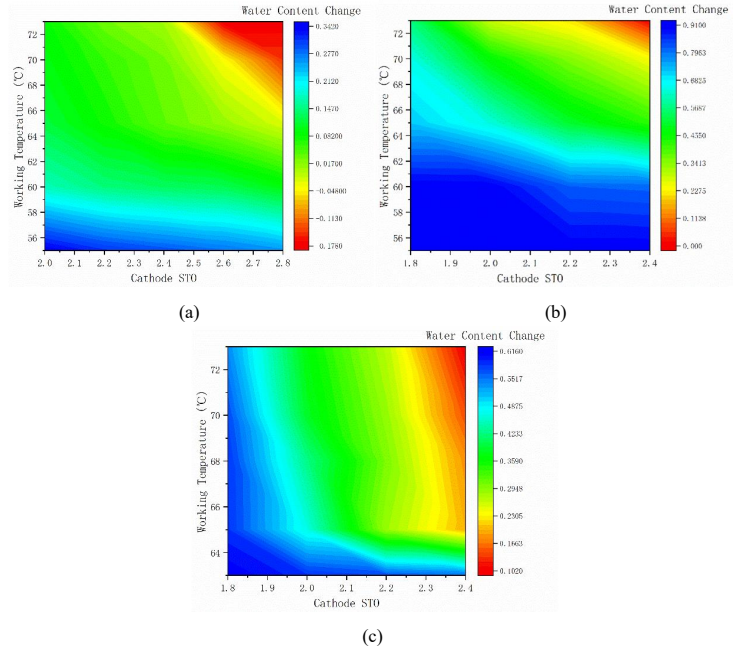
$$x^* = x - \mu\sigma$$

13

Figure 7: Comparison chart of internal water content of fuel cell system under different conditions (a:120A; b:210A; c:300A)

Table 2 shows the result of analysis: Similar to the phenomenon described above, the impact of the working temperature is more significant when load current is on 120A and 210A; while the impact of the air metering ratio is more significant when load current is 300A. Reason for this phenomenon may be the air metering ratio related to the load current. Under different load currents, the air metering ratio changes the same magnitude, but the change in air flow is different. Since the fuel cell system needs to rely on high-speed high-temperature gas to carry the water out, the higher the load current, the more significant the impact of the air metering ratio.

Therefore, to maintain the long-term stable operation of the fuel cell system, appropriate operating conditions need to be selected. The following principles should be considered when choosing:

Table 2: Regression analysis under different load current

Load current(A)	Temperature ratio regression coefficient	Air metering ratio regression coefficient
120	-0.8469	-0.4145
210	-0.9341	-0.4347
300	-0.4637	-0.7618

- The fuel cell system should be in a normal state under this condition;

- In the actual operation process, there are certain fluctuations in the working temperature and air metering ratio. The fluctuation range of the working temperature is about $\pm 2°C$, and the fluctuation range of the air metering ratio is about± 0.1, so the selected conditions should make the points within the fluctuation range in a normal state;

- A larger air metering ratio and a lower working temperature will cause additional consumption of the auxiliary system, so try to choose working conditions with a low air metering ratio and a high working temperature.

As shown in Fig 8, 120A/67$°C$/2.15, 210A/68$°C$/2.15, 300A/70$°C$/2.05 are selected as the appropriate operating conditions under each load current. Next, comparing the rate
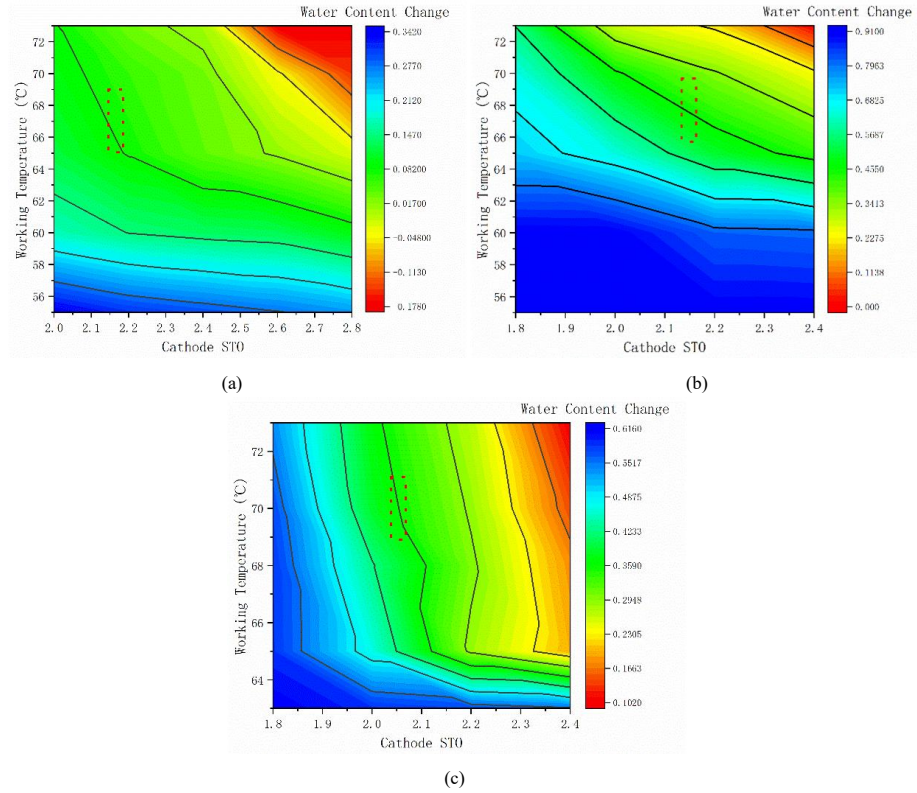

Figure 8: Selection of fuel cell OS operating environment (Working environment surrounded by dots, a:120A; b:210A; c:300A)

of change of the water content inside the fuel cell system under different load currents.

From Table 3, it can be seen that as the load current increases, the rate of change of the water content inside the fuel cell system increases to some extent, but the increase is not large. This may be because the higher the load current of the fuel cell, the more

Table 3: Statistical table of the change rate of internal water content of different load currents

Load current(A)	maximum	minimum	range	average	variance
120	0.342	-0.177	0.519	0.086	0.019
210	0.909	0.009	0.900	0.562	0.067
300	0.615	0.103	0.512	0.402	0.028

water flow is generated, so the water accumulated inside correspondingly increases. In addition, it was found that when the load current is 210A, the range is larger compared to 120A and 300A. Correspondingly, the fuel cell system cannot operate stably under the conditions of 210A/55°C/1.6 and 210A/55°C/1.8. This further reflects the connection between the rate of change of the internal water content of the fuel cell system and the water content fault.

However, the above calculation method can only calculate the absolute value of the water content inside the fuel cell system. The output performance of the fuel cell in actual operation is related to the working temperature, intake pressure, and air metering ratio. To find the most suitable working conditions under each load current, it is necessary to establish a fuel cell stack model, and study the correlation between the difference between the actual output and theoretical output of the fuel cell stack under different conditions and the absolute value of the water content inside the fuel cell system.

4. Conclusion

Different conditions and the absolute value of the water content inside the fuel cell system.

This study investigates the water content state of the high-power fuel cell system and constructs a water balance model. Initially, to authenticate this model, a tail gas water content detection apparatus centered on condensation was designed and established, based on the original high-power fuel cell system. Subsequently, control variable experiments involving three factors, namely, working temperature, air metering ratio, and load current, were executed to measure the water flow rate emanating from the air side and hydrogen side of the fuel cell system during steady-state operation. The experimental outcomes are as follows:

1 Under larger air metering ratios, elevated coolant inlet temperatures, and higher load currents, the water content in the exhaust gas on the air side is higher; conversely, under smaller air metering ratios, lower coolant inlet temperatures, and higher load currents, the water content in the exhaust gas on the hydrogen side is higher.

2 Under the same load current, as the working temperature and air metering ratio escalate, the rate of change of the water content inside the fuel cell system progressively decreases. However, the degree of influence of working temperature and air metering ratio on the rate of change of the water content inside the fuel cell

system slightly varies. When the load current is 120A and 210A, the influence of working temperature is more pronounced; whereas, when the load current is 300A, the influence of the air metering ratio is more evident.

3 With the amplification of load current, the rate of change of the water content inside the fuel cell system somewhat increases, but the increase is not substantial. Simultaneously, the range of the rate of change of the internal water content at 210A is greater than that at 120A and 300A, and the corresponding fuel cell system cannot operate stably under the conditions of $210A/55°C/1.6$ and $210A/55°C/1.8$. This further substantiates the correlation between the rate of change of the internal water content of the fuel cell system and the water content fault.

In conclusion, the water balance model can effectively predict the water content inside the fuel cell system. The experimental results provide a reference for the water content detection of high-power fuel cell systems. The water content status of the fuel cell system can be detected by monitoring the tail gas water volume. The results of this study can provide a theoretical basis for the water content detection of high-power fuel cell systems and can be used as a reference for the operation and maintenance of high-power fuel cell systems.

References

[1] O. Z. Sharaf, M. F. Orhan, An overview of fuel cell technology: Fundamentals and applications, Renewable and Sustainable Energy Reviews 32 (2014) 810–853. `doi:10.1016/j.rser.2014.01.012`.

[2] J. Shen, L. Xu, H. Chang, Z. Tu, S. H. Chan, Partial flooding and its effect on the performance of a proton exchange membrane fuel cell 207 112537. `doi:10.1016/j.enconman.2020.112537`.

[3] T. Ous, C. Arcoumanis, Degradation aspects of water formation and transport in proton exchange membrane fuel cell: A review 240 558–582. `doi:10.1016/j.jpowsour.2013.04.044`.

[4] F. Xiao, T. Chen, Z. Gan, R. Zhang, The influence of external operating conditions on membrane drying faults of proton-exchange membrane fuel cells 285 128787. `doi:10.1016/j.energy.2023.128787`.

[5] T. W. Patterson, R. M. Darling, Damage to the Cathode Catalyst of a PEM Fuel Cell Caused by Localized Fuel Starvation, Electrochem. Solid-State Lett. 9 (4) (2006) A183. `doi:10.1149/1.2167930`.

[6] T. Chu, M. Xie, Y. Yu, B. Wang, D. Yang, B. Li, P. Ming, C. Zhang, Experimental study of the influence of dynamic load cycle and operating parameters on the durability of PEMFC, Energy 239 (2022) 122356. `doi:10.1016/j.energy.2021.122356`.

[7] J. H. Ohs, U. Sauter, S. Maass, D. Stolten, Modeling hydrogen starvation conditions in proton-exchange membrane fuel cells, Journal of Power Sources 196 (1) (2011) 255–263. `doi:10.1016/j.jpowsour.2010.06.038`.

[8] M. Kuracina, J. Fiala, M. Soldán, Study of Selected Characteristics of a Dry Cell Hydrogen Generator in Conditions of Long Term Operation, AMR 887-888 (2014) 985–988. `doi:10.4028/www.scientific.net/AMR.887-888.985`.

[9] F. Jia, L. Guo, H. Liu, Mitigation strategies for hydrogen starvation under dynamic loading in proton exchange membrane fuel cells, Energy Conversion and Management 139 (2017) 175–181. `doi:10.1016/j.enconman.2017.02.051`.

[10] H. Yuan, H. Dai, X. Wei, P. Ming, Model-based observers for internal states estimation and control of proton exchange membrane fuel cell system: A review, Journal of Power Sources 468 (2020) 228376. `doi:10.1016/j.jpowsour.2020.228376`.

[11] H. Fu, J. Shen, L. Sun, K. Y. Lee, Fuel cell humidity modeling and control using cathode internal water content, International Journal of Hydrogen Energy 46 (15) (2021) 9905–9917. `doi:10.1016/j.ijhydene.2020.04.283`.

[12] R. Taccani, N. Zuliani, Effect of flow field design on performances of high temperature PEM fuel cells: Experimental analysis, International Journal of Hydrogen Energy 36 (16) (2011) 10282–10287. `doi:10.1016/j.ijhydene.2010.10.026`.

[13] P. E. Dodds, I. Staffell, A. D. Hawkes, F. Li, P. Grünewald, W. McDowall, P. Ekins, Hydrogen and fuel cell technologies for heating: A review, International Journal of Hydrogen Energy 40 (5) (2015) 2065–2083. `doi:10.1016/j.ijhydene.2014.11.059`.

[14] W. Sun, B. A. Peppley, K. Karan, Modeling the Influence of GDL and flow-field plate parameters on the reaction distribution in the PEMFC cathode catalyst layer, Journal of Power Sources 144 (1) (2005) 42–53. `doi:10.1016/j.jpowsour.2004.11.035`.

[15] N. Yousfi Steiner, D. Hissel, P. Moçotéguy, D. Candusso, Diagnosis of polymer electrolyte fuel cells failure modes (flooding & drying out) by neural networks modeling, International Journal of Hydrogen Energy 36 (4) (2011) 3067–3075. `doi:10.1016/j.ijhydene.2010.10.077`.

[16] B. Chen, W. Ke, M. Luo, J. Wang, Z. Tu, M. Pan, H. Zhang, X. Liu, W. Liu, Operation characteristics and carbon corrosion of PEMFC (Proton exchange membrane fuel cell) with dead-ended anode for high hydrogen utilization, Energy 91 (2015) 799–806. `doi:10.1016/j.energy.2015.08.083`.

[17] I. S. Hussaini, C.-Y. Wang, Visualization and quantification of cathode channel flooding in PEM fuel cells, Journal of Power Sources 187 (2) (2009) 444–451. `doi:10.1016/j.jpowsour.2008.11.030`.

[18] D. Lee, J. Bae, Visualization of flooding in a single cell and stacks by using a newly-designed transparent PEMFC, International Journal of Hydrogen Energy 37 (1) (2012) 422–435. doi:10.1016/j.ijhydene.2011.09.073.

[19] N. Pekula, K. Heller, P. Chuang, A. Turhan, M. Mench, J. Brenizer, K. Ünlü, Study of water distribution and transport in a polymer electrolyte fuel cell using neutron imaging, Nuclear Instruments and Methods in Physics Research Section A: Accelerators, Spectrometers, Detectors and Associated Equipment 542 (1-3) (2005) 134–141. doi:10.1016/j.nima.2005.01.090.

[20] T. Trabold, J. Owejan, D. Jacobson, M. Arif, P. Huffman, In situ investigation of water transport in an operating PEM fuel cell using neutron radiography: Part 1 – Experimental method and serpentine flow field results, International Journal of Heat and Mass Transfer 49 (25-26) (2006) 4712–4720. doi:10.1016/j.ijheatmasstransfer.2006.07.003.

[21] X. G. Yang, F. Y. Zhang, A. L. Lubawy, C. Y. Wang, Visualization of Liquid Water Transport in a PEFC, Electrochem. Solid-State Lett. 7 (11) (2004) A408. doi:10.1149/1.1803051.

[22] H. Li, Y. Tang, Z. Wang, Z. Shi, S. Wu, D. Song, J. Zhang, K. Fatih, J. Zhang, H. Wang, Z. Liu, R. Abouatallah, A. Mazza, A review of water flooding issues in the proton exchange membrane fuel cell, Journal of Power Sources 178 (1) (2008) 103–117. doi:10.1016/j.jpowsour.2007.12.068.

[23] B. Legros, P.-X. Thivel, Y. Bultel, R. Nogueira, First results on PEMFC diagnosis by electrochemical noise, Electrochemistry Communications 13 (12) (2011) 1514–1516. doi:10.1016/j.elecom.2011.10.007.

[24] J. Wu, X. Ziyuan, H. Wang, M. Blanco, J. Martin, J. Zhang, Diagnostic tools in PEM fuel cell research: Part IIPhysical/chemical methods, International Journal of Hydrogen Energy 33 (6) (2008) 1747–1757. doi:10.1016/j.ijhydene.2008.01.020.

[25] Y. Li, P. Pei, Z. Wu, H. Xu, D. Chen, S. Huang, Novel approach to determine cathode two-phase-flow pressure drop of proton exchange membrane fuel cell and its application on water management, Applied Energy 190 (2017) 713–724. doi:10.1016/j.apenergy.2017.01.010.

[26] P. Moçotéguy, B. Ludwig, D. Beretta, T. Pedersen, Study of the impact of water management on the performance of PEMFC commercial stacks by impedance spectroscopy 45 (33) 16724–16737. doi:10.1016/j.ijhydene.2020.04.139.

[27] S. Laribi, K. Mammar, M. Hamouda, Y. Sahli, Impedance model for diagnosis of water management in fuel cells using artificial neural networks methodology 41 (38) 17093–17101. doi:10.1016/j.ijhydene.2016.07.099.

[28] Z. Tang, Q.-A. Huang, Y.-J. Wang, F. Zhang, W. Li, A. Li, L. Zhang, J. Zhang, Recent progress in the use of electrochemical impedance spectroscopy for the measurement, monitoring, diagnosis and optimization of proton exchange membrane fuel cell performance, Journal of Power Sources 468 (2020) 228361. `doi: 10.1016/j.jpowsour.2020.228361`.

[29] N. Fouquet, C. Doulet, C. Nouillant, G. Dauphin-Tanguy, B. Ould-Bouamama, Model based PEM fuel cell state-of-health monitoring via ac impedance measurements, Journal of Power Sources 159 (2) (2006) 905–913. `doi:10.1016/j. jpowsour.2005.11.035`.

[30] Y. Jiang, X. Yang, P. Liang, P. Liu, X. Huang, Microbial fuel cell sensors for water quality early warning systems: Fundamentals, signal resolution, optimization and future challenges, Renewable and Sustainable Energy Reviews 81 (2018) 292–305. `doi:10.1016/j.rser.2017.06.099`.

[31] G. Dotelli, R. Ferrero, P. Gallo Stampino, S. Latorrata, S. Toscani, Combining Electrical and Pressure Measurements for Early Flooding Detection in a PEM Fuel Cell, IEEE Trans. Instrum. Meas. 65 (5) (2016) 1007–1014. `doi:10.1109/ TIM.2015.2490999`.

[32] M. Miller, A. Bazylak, A review of polymer electrolyte membrane fuel cell stack testing, Journal of Power Sources 196 (2) (2011) 601–613. `doi:10.1016/j. jpowsour.2010.07.072`.

[33] V. M. Nagulapati, S. S. Kumar, V. Annadurai, H. Lim, Machine learning based fault detection and state of health estimation of proton exchange membrane fuel cells, Energy and AI 12 (2023) 100237. `doi:10.1016/j.egyai.2023.100237`.

[34] I. Verhaert, S. Verhelst, G. Janssen, G. Mulder, M. De Paepe, Water management in an alkaline fuel cell 36 (17) 11011–11024. `doi:10.1016/j.ijhydene.2011. 05.172`.

[35] X. Zhao, R. Wang, Y. Zhang, D. Hao, Z. Yang, Study on Water Transport Mechanisms of the PEMFC Based on a Visualization Platform and Water Balance Model, International Journal of Chemical Engineering 2021 (2021) 1–12. `doi:10.1155/2021/9298305`.

[36] C. Bonnet, S. Didierjean, N. Guillet, S. Besse, T. Colinart, P. Carré, Design of an 80kWe PEM fuel cell system: Scale up effect investigation 182 (2) 441–448. `doi:10.1016/j.jpowsour.2007.12.100`.

[37] M. Ji, Z. Wei, A Review of Water Management in Polymer Electrolyte Membrane Fuel Cells 2 (4) 1057–1106. `doi:10.3390/en20401057`.

[38] M. Shojayian, E. Kjeang, Simulation of cathode catalyst durability under fuel cell vehicle operation –Effects of stack size and temperature 591 233820. `doi:10. 1016/j.jpowsour.2023.233820`.

[39] E. I. Altman, Predicting financial distress of companies: revisiting the z-score and zeta® models, in: Handbook of research methods and applications in empirical finance, Edward Elgar Publishing, 2013, pp. 428–456.

[40] D. Camska, Predicting financial distress of companies in the agricultural sector., in: Economic Science for Rural Development Conference Proceedings, no. 30, 2013.